THE JOURNAL OF PHYSICAL CHEMISTRY Letters

Letter

Cite This: J. Phys. Chem. Lett. 2019, 10, 4177−4184

pubs.acs.org/JPCL

Improved Doping and Emission Efficiencies of Mn-Doped $CsPbCl_3$ Perovskite Nanocrystals via Nickel Chloride

Ke Xing,[†] Xi Yuan,*[,†] Yu Wang,[†] Ji Li,[†] Yunjun Wang,[‡] Yi Fan,[§] Long Yuan,[†] Kai Li,[∥] Zhijian Wu,[∥] Haibo Li,*[,†] and Jialong Zhao*[,†,⊥]

[†]Key Laboratory of Functional Materials Physics and Chemistry of the Ministry of Education, Jilin Normal University, Changchun 130103, China

[‡]Suzhou Xingshuo Nanotech Co., Ltd. (Mesolight), Suzhou 215123, China

[§]State Key Laboratory of Luminescence and Applications, Changchun Institute of Optics, Fine Mechanics and Physics, Chinese Academy of Sciences, Changchun 130033, China

[∥]State Key Laboratory of Rare Earth Resource Utilization, Changchun Institute of Applied Chemistry, Chinese Academy of Sciences, Changchun 130022, China

[⊥]Key Laboratory of Preparation and Application of Environmental Friendly Materials, Ministry of Education, Jilin Normal University, Changchun 130103, China

Supporting Information

ABSTRACT: It is challenging to improve the emission efficiency of Mn-doped $CsPbCl_3$ ($Mn:CsPbCl_3$) nanocrystals (NCs) because the excellent optical performances are dependent on high doping efficiency and few defects and traps. Steady-state and time-resolved photoluminescence (PL) spectroscopies were used to investigate the luminescence properties of $Mn:CsPbCl_3$ NCs with different Mn doping levels synthesized in the presence of nickel chloride. The doping efficiency of Mn ions in $Mn:CsPbCl_3$ NCs was greatly enhanced in the presence of $NiCl_2$, and the PL wavelength of Mn^{2+} ions was tuned from 594 to 638 nm by varying the concentration of dopant Mn from 0.11% to 15.25%. The high emission quantum yields of $Mn:CsPbCl_3$ NCs with orange and red emissions peaked at 600 and 620 nm in hexane were 70% and 39%, respectively. The improvement in doping and emission efficiencies of Mn^{2+} was attributed to the enhanced formation energies of the Mn doping under the Mn and Ni codoped configuration and the resulting reduction of defects and traps in $Mn:CsPbCl_3$ NCs with incorporation of Ni^{2+} ions.

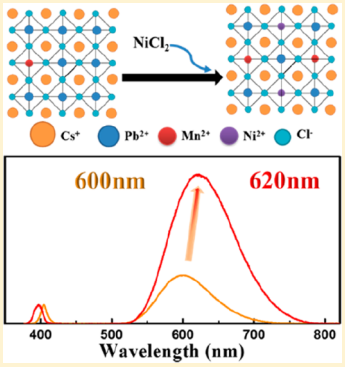

Mn-doped perovskite nanocrystals (NCs) with broad yellow-orange emission have exhibited potential application in white light-emitting diodes (LEDs) since the first doping of Mn^{2+} into perovskite was reported in 2016.[1,2] The yellow-orange emission in Mn-doped $CsPbCl_3$ ($Mn:CsPbCl_3$) NCs comes from the transfer of exciton energy to Mn d-states, leading to the d−d transition ($^4T_1 \rightarrow {}^6A_1$).[1−19] Mn-doped $CsPbCl_3$ NCs with yellow−orange emission (~590−600 nm) from isolated Mn^{2+} ions show high photoluminescence quantum yields (PL QYs) up to about 60%, while the ones with red emission (~620−630 nm) partly from Mn−Mn dimers have relatively low PL QYs of as high as about 10%.[9,10,19] The tuning of Mn^{2+} emission from yellow to red is achieved by enhancing the concentration of dopant Mn to form Mn−Mn dimers in NCs.[9,10] However, the reduction in PL QY of red Mn^{2+} emission is considered to originate from nonradiative recombination pathways due to the Mn−Mn dimers and many defects and traps in NCs under high concentration Mn doping at high reaction temperature. Therefore, suppressing the formation of high-density defect and trap states as nonradiative centers in NCs is an efficient strategy to improve red Mn^{2+} emission for high-performance white LEDs.[20−23]

The PL QYs of intrinsic and doped $CsPbCl_3$ NCs have been greatly enhanced by two main strategies.[24−27] The first one is doping metal ions into $CsPbCl_3$ lattices to realize the doping-induced structure order in the lattice based on a high-temperature hot-injection route. Sun et al. used Ni^{2+} ion doping to enhance formation energies of defects in the $CsPbCl_3$ lattice, obtaining near-unity PL QY.[28] Similarly, the doping of other metal cations such as Cd^{2+} and Cu^{2+} was used to significantly boost the efficiency of band-edge PL.[29−31] The second strategy is adding metal chlorides into $CsPbCl_3$ NC solutions to passivate the NC surface and eliminate the defect and trap centers at or near the surface based on the room-temperature postsynthetic surface treatment.[32−34] Recently, the improved emission efficiency of $Mn:CsPbCl_3$ NCs with addition of $CuCl_2$ has also been demonstrated by maximizing the doping efficiency in NCs and minimizing the chloride

Received: June 3, 2019
Accepted: July 10, 2019
Published: July 10, 2019

DOI: 10.1021/acs.jpclett.9b01588
J. Phys. Chem. Lett. 2019, 10, 4177−4184

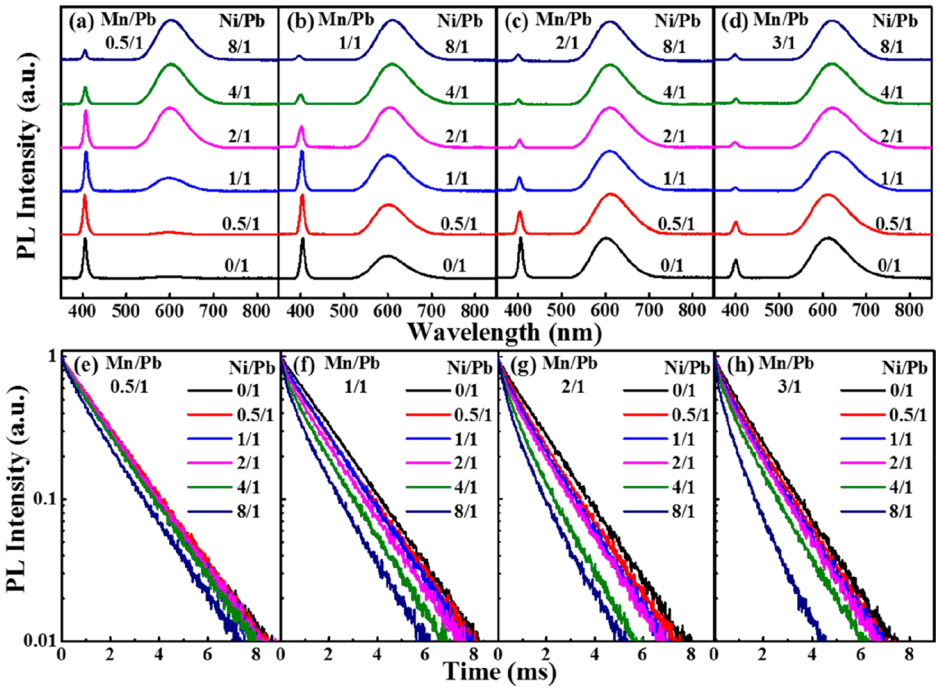

Figure 1. Steady-state and time-resolved PL spectra of Mn:$CsPbCl_3$ NCs with various Mn/Pb (from 0.5/1 to 3/1) and Ni/Pb molar ratios (from 0/1 to 8/1).

deficiency.[19] Therefore, doping of metal ions like Ni, Cu, Fe, Co, etc. is an effective way to enhance the optical properties of intrinsic and doped perovskite.[35−46]

The concentration quenching is a problem of phosphor application in lighting and display.[47−53] For high Mn doping levels, energy transfer among Mn^{2+} or between Mn^{2+} and defects can lead to concentration-induced PL quenching and lifetime shortening. Therefore, studying temperature-dependent lifetimes of Mn^{2+} emission is very important to understand the concentration-quenching PL mechanism of the Mn:$CsPbCl_3$ NCs for application of white LEDs.[54,55]

In this Letter, Mn doping concentration-dependent optical and structural properties of Mn:$CsPbCl_3$ NCs prepared at 190 °C in the presence and absence of nickel chloride were investigated via using steady-state and time-resolved PL spectroscopies and synchrotron radiation X-ray diffraction (XRD). Effects of Ni^{2+} ions on the doping and emission efficiencies of Mn^{2+} in Mn:$CsPbCl_3$ NCs were studied, and the tuning of Mn^{2+} emission wavelength was examined by changing the Mn doping concentration. The improvement in doping and emission efficiencies of Mn:$CsPbCl_3$ NCs with orange and red emissions peaked at 600 and 620 nm in hexane were revealed.

Steady-state and time-resolved PL spectra of Mn doping concentration-varied Mn:$CsPbCl_3$ NCs synthesized with different molar ratios of Mn/Pb (0.25/1, 0.5/1, 1/1, 2/1, 3/1, and 4/1) and Ni/Pb (0/1, 0.5/1, 1/1, 2/1, 4/1, and 8/1) at 190 °C are shown in Figures 1 and S1. The corresponding absorption spectra are displayed in Figure S2. The synthesis and characterization methods of these Mn:$CsPbCl_3$ NCs are described in the Supporting Information. No new absorption band is found after the introduction of Ni^{2+}, suggesting that the nickel doping has a weak effect on the electronic structure of $CsPbCl_3$, as seen in Figure S2. With increasing the amount of Mn^{2+} and Ni^{2+}, the band-edge absorption peaks exhibit broadening and blue-shift, which reflect the statistical fluctuation of the number of Mn/Ni doped into $CsPbCl_3$ and the effect of Mn- and Ni-alloying on the host band gap.[1,9,28] As is well-known, Mn:$CsPbCl_3$ NCs exhibit a broad Mn^{2+} PL band at about 600 nm and a sharp exciton emission at about 400 nm at room temperature.[1,2] The pristine Mn:$CsPbCl_3$ NCs synthesized only with a Mn/Pb ratio of 0.5/1 show a weak Mn^{2+} emission at 594 nm and a strong exciton PL band at 405 nm, as seen in Figure 1a. The Mn^{2+} emission intensity clearly increases with increasing Ni/Pb ratio from 0.5/1 to 8/1; meanwhile, the exciton PL band intensity decreases because of energy transfer from the exciton to Mn.[1,2] In addition, the Mn^{2+} emission peak slightly shifts to the red from 594 to 602 nm after increasing the amount of $NiCl_2$. The Mn:$CsPbCl_3$ NCs with a 0.5/1 ratio of Mn to Pb show a single-exponential decay for Mn^{2+} emission, as shown in Figure 1e. The Mn^{2+} decay almost remains constant as the ratio of Ni to Pb increases from 0.5 to 4/1, except 8/1. Further, the Mn:$CsPbCl_3$ NCs with a 1/1, 2/1, 3/1, and 4/1 ratio of Mn to Pb show a significantly enhanced Mn^{2+} emission band, accompanied by a clearly increased Mn^{2+} emission redshift from 599 to 609 nm, 601 to 610 nm, 610 to 621 nm, and 611 to 638 nm, respectively, and a clearly decreased exciton emission band as the ratio of Ni to Pb increases, as shown in Figures 1b−d and S1b. The redshift of Mn^{2+} emission is usually due to formation of Mn−Mn dimers, leading to a shortening of Mn^{2+} emission lifetime.[9,10] On the other hand, the time-resolved PL spectra of Mn^{2+} in pristine Mn:$CsPbCl_3$ NCs only with 1/1 and 2/1 ratios of Mn to Pb clearly show a single-exponential decay for Mn^{2+} emission, as shown in Figure 1f,g. The PL decay gradually becomes multiexponential with a reduced lifetime with enhancing the ratio of Ni/Pb. The Mn:$CsPbCl_3$ NCs with 3/1 and 4/1 ratio of Mn to Pb have a reduced multiexponential decay with increasing Ni/Pb ratio, as seen in Figures 1h and S1d. Therefore, the significant redshift and lifetime reduction of Mn^{2+} emissions with increasing Ni/

DOI: 10.1021/acs.jpclett.9b01588
J. Phys. Chem. Lett. 2019, 10, 4177−4184

Pb ratio indicate improved Mn doping efficiency in Mn:$CsPbCl_3$ NCs with increasing addition of $NiCl_2$.

The PL QYs and lifetimes of Mn^{2+} in Mn:$CsPbCl_3$ NCs with different molar ratios of Mn/Pb (0.25/1,0.5/1, 1/1, 2/1, 3/1, and 4/1) and Ni/Pb (0/1, 0.5/1, 1/1, 2/1, 4/1, and 8/1) are shown in Figures 2 and S3. In our previous work, it is found

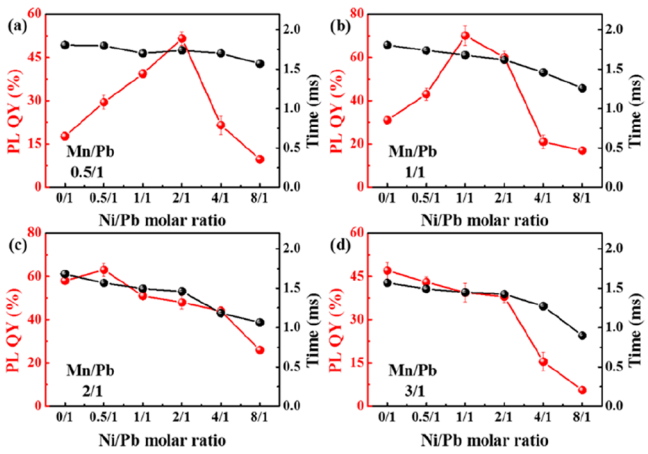

Figure 2. PL QYs and lifetimes of Mn^{2+} in Mn:$CsPbCl_3$ NCs with different molar ratios of Mn/Pb (from 0.5/1 to 3/1) and Ni/Pb (from 0/1 to 8/1).

that the efficiency of Mn^{2+} emission in Mn-doped $CsPbCl_3$ NCs gradually enhances as the Mn doping concentration increases, reaches the maximum of about 60% when the Mn/Pb is 2/1, and then drops after the Mn−Mn dimers occur.[9] The PL QY of Mn^{2+} ions in the NCs with initial Mn/Pb ratio of 0.5/1 increases with increasing the Ni/Pb ratio from 0 to 2/1 and reaches the maximum value of 52% and then rapidly decreases to 11% with continually increasing the Ni/Pb ratio to 8/1, as shown in Figure 2a. However, the PL lifetime of Mn^{2+} slightly decreases from 1.80 to 1.57 ms with increasing the ratio of Ni/Pb from 0 to 8/1. The PL QY of Mn^{2+} in Mn:$CsPbCl_3$ NCs (Mn/Pb of 1/1) increases with increasing the Ni/Pb from 0 to 1/1, reaches the highest value of 70%, and then clearly drops to 17% with increasing the Ni/Pb ratio to 8/1, as shown in Figure 2b. It is noted that the PL lifetime of Mn^{2+} varies only from 1.80 to 1.25 ms with enhancing the ratio of Ni/Pb ratio from 0/1 to 8/1. The PL lifetime of Mn^{2+} ions is 1.67 ms for the Mn:$CsPbCl_3$ NCs with the highest PL QY, which is slightly lower than the longest one of about 1.80 ms in pure Mn:$CsPbCl_3$ NCs.[9,56] The efficiency of Mn^{2+} emission in Mn:$CsPbCl_3$ NCs (Mn/Pb of 2/1) has the highest PL QY of 65% when the Ni/Pb ratio is 0.5/1, as shown in Figure 2c. Then the PL QY is reduced with increasing the Ni/Pb ratio while their PL lifetime decreases from 1.68 to 1.01 ms. In Figures 2d and S3b, the efficiency of Mn^{2+} emission in Mn:$CsPbCl_3$ NCs (Mn/Pb of 3/1 and 4/1) has the highest PL QY of 47% and 44% at the Ni/Pb ratio of 0/1, and slowly reduced PL QYs are observed with increasing the Ni/Pb ratio while their PL lifetimes decrease from 1.56 to 0.90 ms and 1.64 to 0.30 ms, respectively. In the presence of $NiCl_2$, the high-efficiency Mn doping results in the improved QYs of 600 and 620 nm Mn^{2+} emissions up to 70% and 39%, respectively, in Mn:$CsPbCl_3$ NCs synthesized with codoped Ni^{2+} at the low temperature of 190 °C, compared with 60% (600 nm) and 10% (620 nm) of pure Mn:$CsPbCl_3$ NCs,[9,10,19] 20−40% of Mn:$CsPbCl_3$ nanoplatelets (~600 nm),[57,58] 61% of Mn:L_2PbBr_4 layered perovskite (~600 nm),[59] and 16 ± 4% of Mn:$Cs_2AgInCl_6$ NCs (620 nm).[60] On the other hand, it is noted that the efficiency and lifetime of Mn^{2+} emission are dependent not only on the Mn/Pb ratio but also on the Ni/Pb molar ratio. The PL QY of Mn^{2+} clearly increases with increasing Ni/Pb ratio when the low Mn/Pb ratios are 0.25/1, 0.5/1, 1/1, and 2/1. However, their lifetime of Mn^{2+} emission is smaller than the longest PL lifetime of 1.80 ms that we obtained. In our previous work, the shortening of Mn^{2+} PL lifetimes was related to formation of Mn−Mn pairs or defect and trap states, leading to a decrease of Mn^{2+} PL QY.[9,10] Thus, the clear decrease in the lifetime of Mn^{2+} emission in Mn-doped $CsPbCl_3$ NCs with the highest PL QYs might be attributed to the change in the local environment around the Mn^{2+} ion with interaction of Ni^{2+} ions because the lifetime of Mn^{2+} emission is dependent on Ni-doping concentration.

Figure 3 shows the Mn doping concentration dependence of Mn^{2+} PL QYs and wavelengths in Mn-doped $CsPbCl_3$ NCs

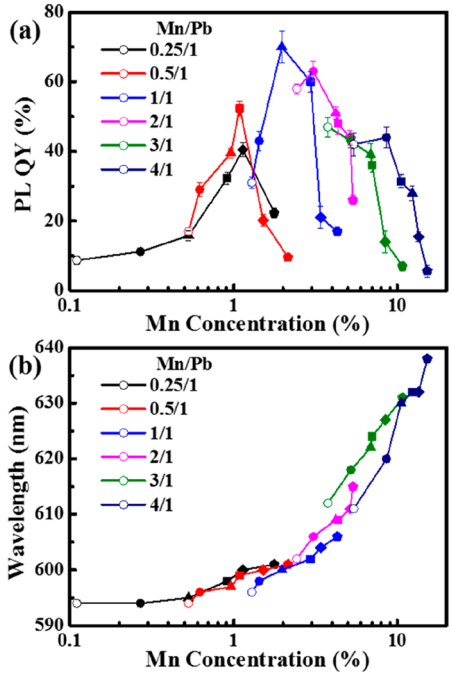

Figure 3. Mn doping concentration-dependent QYs (a) and wavelengths (b) of Mn^{2+} emissions in Mn:$CsPbCl_3$ NCs with different molar ratios of Mn/Pb (0.25/1, 0.5/1, 1/1, 2/1, 3/1, and 4/1) and Ni/Pb [0/1 (empty circles), 0.5/1 (solid circles), 1/1 (solid triangles), 2/1 (solid squares), 4/1 (solid diamonds), and 8/1 (solid pentagons)].

with different molar ratios of Mn/Pb (0.25/1, 0.5/1, 1/1, 2/1, 3/1, and 4/1) and Ni/Pb (0/1, 0.5/1, 1/1, 2/1, 4/1, and 8/1). The corresponding actual doping concentrations of Mn^{2+} and Ni^{2+} are summarized in Tables 1 and S1. As shown in Table 1, the Mn^{2+} and Ni^{2+} concentrations increase with increasing the feed ratio of Ni/Pb. The Mn:$CsPbCl_3$ NCs clearly show improved Mn doping efficiencies in the presence of $NiCl_2$ and maximized emission efficiencies for the corresponding various Ni/Pb ratios (Figure 3). The Mn:$CsPbCl_3$ NCs doped with Mn^{2+} and Ni doping concentrations of 1.97% and 3.18%, respectively, have the highest PL QY of 70%, which is consistent with Mn(II)-doped $CsPbCl_3$ ones with a PL QY of 68% because of the maximized doping efficiency in the presence of $CuCl_2$.[19] Further, it is worth noting that high-

DOI: 10.1021/acs.jpclett.9b01588
J. Phys. Chem. Lett. 2019, 10, 4177−4184

Table 1. Doping Concentrations of Mn^{2+} (Relative to the Sum of Pb^{2+} and Ni^{2+} Ions) and Ni^{2+} (Relative to the Sum of Pb^{2+} and Mn^{2+}) in Mn-Doped $CsPbCl_3$ NCs Synthesized with Different Molar Ratios of Mn/Pb (0.5/1, 1/1, 2/1, and 3/1) and Ni/Pb (0/1, 0.5/1, 1/1, 2/1, 4/1, and 8/1) Measured by ICP-MS

	Mn/Pb							
	0.5/1		1/1		2/1		3/1	
Ni/Pb	Mn	Ni	Mn	Ni	Mn	Ni	Mn	Ni
0/1	0.53%	0	1.29%	0	2.43%	0	3.76%	0
0.5/1	0.62%	1.98%	1.43%	2.01%	3.07%	2.12%	5.21%	2.10%
1/1	0.96%	3.06%	1.97%	3.18%	4.21%	3.16%	6.87%	3.11%
2/1	1.09%	4.08%	2.96%	4.14%	4.34%	4.20%	7.01%	4.21%
4/1	1.52%	11.71%	3.41%	11.90%	5.15%	11.81%	8.44%	11.89%
8/1	2.15%	19.05%	4.33%	18.17%	5.36%	18.09%	10.78%	17.92%

concentration Mn-doped NCs still have very high PL QYs and long PL lifetimes, compared with the corresponding pristine Mn:$CsPbCl_3$ NCs.[9,10,19] On the other hand, it is clearly observed that Mn^{2+} emission is tuned from 594 to 638 nm by increasing Mn^{2+} concentration from 0.11% to about 15.25%. The PL QYs of excitons in Mn:$CsPbCl_3$ NCs with different molar ratios of Mn/Pb (from 0.25/1 to 4/1) and Ni/Pb (from 0/1 to 8/1) are shown in Table S2. It is found that the PL QYs of excitons are very low (<2%) when the concentrations of Mn^{2+} are high (>5%), which can be attributed to more efficient energy transfer from the exciton to Mn^{2+} and many defects in the NCs.[1,2] In addition, the effects of metal ions such as Fe^{2+} and Co^{2+} ions on optical properties of Mn:$CsPbCl_3$ NCs synthesized at 190 °C were studied in the presence of $CoCl_2$ and $FeCl_2$. The PL spectra, decay curves, QYs, and lifetimes of Mn:$CsPbCl_3$ NCs synthesized with different molar ratios of Mn/Pb (1/1 and 2/1) and Co/Pb and Fe/Pb (0/1, 1/1, 2/1, 4/1) ratios at 190 °C are depicted in Figures S4−S7, and the corresponding Mn doping concentrations are summarized in Table S3. The Mn doping efficiencies in Mn:$CsPbCl_3$ NCs are clearly improved, and under the corresponding Mn/Pb of 1/1, the highest Mn^{2+} emission efficiencies are about 58% and 35% for these NCs synthesized with Co/Pb and Fe/Pb ratios of 1/1, respectively.

The representative transmission electron microscopy (TEM) images of Mn:$CsPbCl_3$ NCs (Mn/Pb of 1/1) without/with Ni doping (Ni/Pb from 0/1 to 8/1) are exhibited in Figure 4a−f. The Mn:$CsPbCl_3$ NCs without Ni doping are uniformly distributed; the average size (cube length) is 10.5 ± 0.8 nm, and the size distributions are also very uniform with average value of 9.7 ± 0.4 and 8.8 ± 0.7 nm at the Ni/Pb ratios 1/1 and 2/1 and become ununiform with significantly reduced average size of 7.4 ± 2.1 and 10.7 ± 3.6 nm at the Ni/Pb ratios of 4/1 and 8/1, respectively. The wide size distribution might result from the effect of high concentration Ni^{2+} ions on NC growth in the reaction solution, causing a significant PL lifetime reduction of Mn^{2+} for the NCs with high Ni/Pb of 4/1 and 8/1 as seen in Figure 2. A high-resolution TEM image shows that the Mn:$CsPbCl_3$ NCs have excellent crystallinity after Ni doping, as seen in Figure 4f. The lattice spacings of about 0.38 and 0.56 nm for 110 and 100 directions of Mn:$CsPbCl_3$ NCs are estimated, consistent with previous reports.[33,61] Figure 4g depicts the X-ray diffraction (XRD) patterns of Mn:$CsPbCl_3$ NCs (Mn/Pb of 1/1) with Ni/Pb ratios of 1/1, 2/1, 4/1, and 8/1 and without (0/1) metal ion doping. The Mn:$CsPbCl_3$ NCs without/with Mn^{2+} and Ni doping have a structure of the parent cubic $CsPbCl_3$ (JCPDS: 75-0411). Two strong diffraction peaks at 15.8° and 31.9° are observed, corresponding to (100) and (200) directions, respectively. The magnified diffraction peaks of Mn:$CsPbCl_3$ NCs show a clear shift to a large angle after addition of $NiCl_2$, meaning the increased doping of Mn^{2+} and/or Ni^{2+}, as depicted in Figure 4h. The broadening of diffraction peaks for doped NCs with a high Ni/Pb ratio is found, perhaps associated with the large size distribution and reduction of the NC size. In addition, compared with diffraction peaks of undoped $CsPbCl_3$ NCs, the Ni doped ones show a small shift to a large angle as seen in Figure S8, indicating the doping of Ni^{2+} in the lattice.

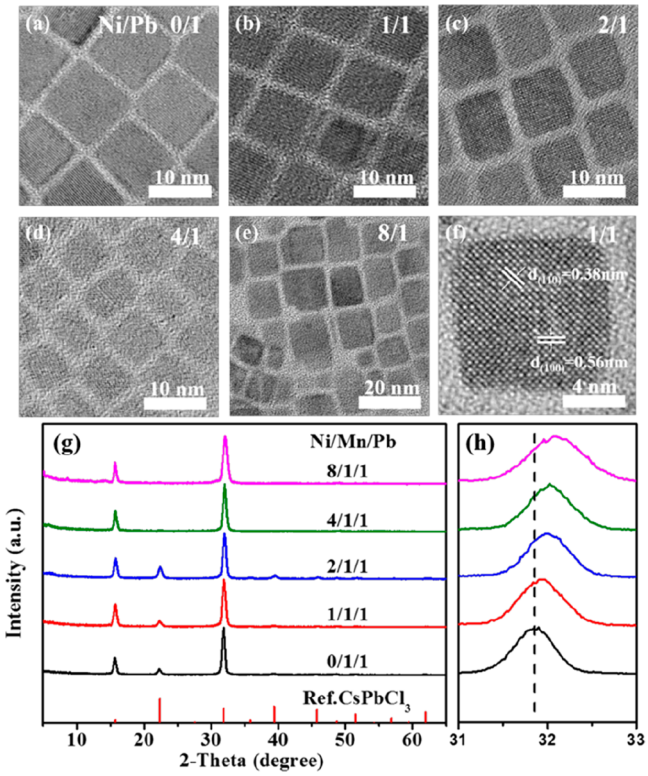

Figure 4. TEM images (a−e) and XRD patterns (g and h) of Mn:$CsPbCl_3$ NCs (Mn/Pb of 1/1) without/with Ni doping (Ni/Pb from 0/1 to 8/1). High-resolution TEM image (f) of typical Mn:$CsPbCl_3$ NCs (Ni/Pb of 1/1).

The synchrotron radiation (λ = 0.434 Å) XRD results of typical Mn-doped $CsPbCl_3$ and Mn and Ni codoped $CsPbCl_3$ NCs are shown in Figure S9. The Rietveld profile refining of synchrotron radiation (λ = 0.434 Å) XRD patterns of the two samples indicates a good fitting. This suggests that Mn and Ni occupy the Pb-site, respectively, with six-coordinated Cl in the

DOI: 10.1021/acs.jpclett.9b01588
J. Phys. Chem. Lett. 2019, 10, 4177−4184

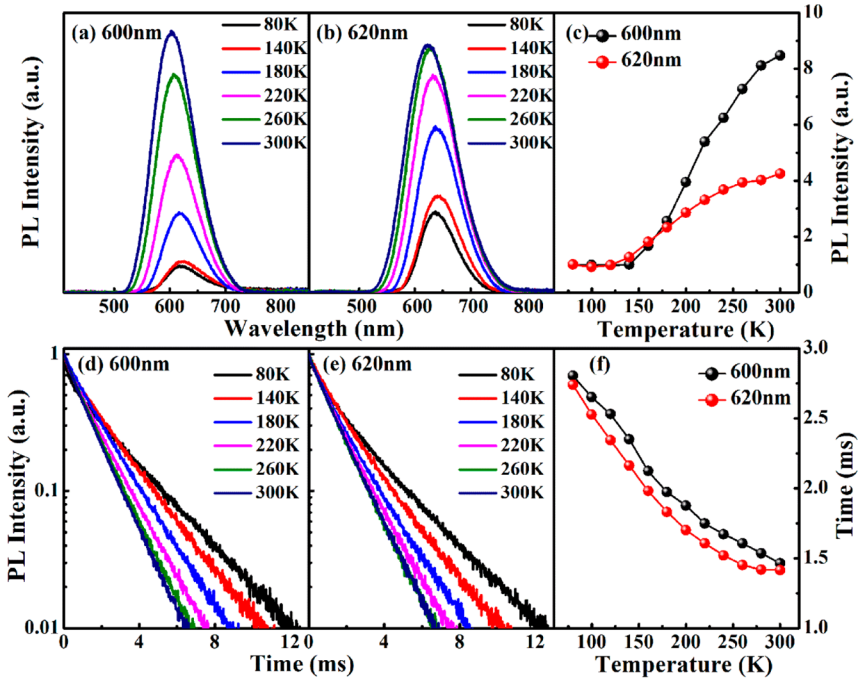

Figure 5. Steady-state and time-resolved PL spectra of 600 nm (a and d) and 620 nm (b and e) Mn^{2+} emissions in Mn:$CsPbCl_3$ NCs synthesized in the presence of $NiCl_2$ and the corresponding PL intensities and lifetimes at various temperatures. PL intensities of Mn^{2+} ions are normalized at 80 K. PL (c) intensities and (f) lifetimes of Mn^{2+} ions with 600 and 620 emissions in Mn:$CsPbCl_3$ NCs with Ni^{2+} incorporation.

as-synthesized NCs, which is consistent with previous reports.[2,10,28,62]

To further understand the effect of Ni, we have employed density functional theory (DFT) to calculate formation energies of the possible Mn^{2+} doping configurations. The formation energy (ΔE_f) is defined as follows: (1) pure $CsPbCl_3$: $\Delta E_f = E_{Mn-CsPbCl_3} - E_{CsPbCl_3} + \mu_{Pb} - \mu_{Mn}$; and (2) Ni-doped configuration: $\Delta E_f = E_{Mn-Ni-CsPbCl_3} - E_{Ni-CsPbCl_3} + \mu_{Pb} - \mu_{Mn}$, where E_{CsPbCl_3}, $E_{Ni-CsPbCl_3}$, and $E_{Ni-Mn-CsPbCl_3}$ are the total energies of pure $CsPbCl_3$, Ni:$CsPbCl_3$, and (Mn,Ni):$CsPbCl_3$, respectively. μ_{Pb} and μ_{Mn} are the chemical potentials of Pb and Mn, respectively, which are estimated by the bulk Pb and Mn, respectively. When ΔE_f is more negative, Mn doping is more favored. For the Ni^{2+} and Mn^{2+} codoped configuration, there are two possible structures: Ni-bulk-1 and -2, as shown in Figure S10. It is found that the doped Ni atom will improve the Mn doping efficiency in some structures (Ni-bulk-2), compared with the pure $CsPbCl_3$.

The partial density of states (PDOSs) for $CsPbCl_3$, Mn:$CsPbCl_3$, and (Mn,Ni):$CsPbCl_3$ are shown in Figure S11. For PDOS of pure $CsPbCl_3$, it is seen that the valence band is mainly constructed by the Cl-2p orbital, while the Pb-6p orbital mainly contributes to the conduction band. Therefore, the electron transition will occur from Cl-2p to Pb-6p. For the Mn-doped configuration, the band gap will be reduced, which makes the electron transition more favorable. Moreover, besides the possible transition pathway in pure $CsPbCl_3$, there will be another two possible electron transition pathways, i.e., Mn-3d to Pb-6p and Cl-2p to Mn-3d. For (Mn,Ni):$CsPbCl_3$, the band gap will be further reduced. It is seen that the impurity band produced by Mn-3d and Ni-3d appears at the band gap, which will improve the possibility for electron transition. Therefore, the Ni has a positive effect in Mn doping, improving the electronic structure.

In order to understand the enhancement mechanism of Mn doping and emission efficiencies in Mn:$CsPbCl_3$ NCs synthesized in the presence of $NiCl_2$, their variable-temperature steady-state and time-resolved PL spectra from 80 to 300 K were measured. The representative PL spectra, decay curves, and corresponding PL intensities and lifetimes of 600 and 620 nm Mn^{2+} emissions at different temperature are shown in Figure 5. The doped NCs were synthesized with Mn/Pb of 1/1 and 3/1, respectively, and Ni/Pb ratio of 1/1 at 190 °C. For comparison, the Mn:$CsPbCl_3$ NCs with the same Mn^{2+} emissions of 600 and 620 nm were prepared with Mn/Pb of 2/1 and 4/1 and without incorporation of Ni^{2+} ions at 190 and 210 °C, respectively; Figure S12 depicts their temperature-dependent PL spectra, decay curves, intensities, and lifetimes. The corresponding PL QYs of the four doped NC samples with various Mn doping concentrations are summarized in Table S4. The PL intensities of Mn^{2+} emissions peaked at 600 and 620 nm with Ni^{2+} incorporation increase as temperature increases from 80 to 300 K (Figure 5a,b), in contrast to those in Mn-doped ZnSe quantum dots.[55] The abnormal PL emission enhancement of Mn^{2+} with increasing temperature is explained by the low exciton-to-Mn^{2+} energy transfer and strongly temperature-dependent exciton lifetimes.[9,12,13] The PL intensities of Mn^{2+} ions with 600 and 620 emissions in Mn:$CsPbCl_3$ NCs with Ni^{2+} incorporation increase with the increase of temperature, as depicted in Figure 5c.[9] In Figure 5d,e, PL decays become short with increasing temperature, which is consistent with thermal quenching.[9,54] The PL lifetimes of Mn^{2+} ions for 600 and 620 emissions in Mn:$CsPbCl_3$ NCs with Ni^{2+} incorporation clearly decrease with increasing temperature, as shown in Figure 5f. Lifetimes of Mn^{2+} ions for the 600 and 620 emission bands are close to each other at the corresponding various temperatures, which are smaller than the difference between 600 and 620 emission bands in the NCs without Ni^{2+} incorporation.[9,19] In general,

DOI: 10.1021/acs.jpclett.9b01588
J. Phys. Chem. Lett. 2019, 10, 4177−4184

the shortening in lifetime of Mn^{2+} emission in Mn:$CsPbCl_3$ NCs with increasing dopant concentration is considered to result from magnetic coupling between Mn−Mn dimers and formed defects/traps near the Mn^{2+} ion.[53−55] This indicates that the lengthening in lifetimes of Mn^{2+} emission at 620 nm in the NCs with Ni^{2+} is attributed to Ni doping-induced structure order in Mn:$CsPbCl_3$ NCs or the surface passivation of Ni^{2+} ions.[27,35,62]

During Mn:$CsPbCl_3$ NC preparation with addition of $NiCl_2$, the transition metal Ni is considered to partly substitute Pb in $CsPbCl_3$ NCs and enhance crystallinity of $CsPbCl_3$ NCs, suppressing the nonradiative recombination,[28,35,62] consistent with our XRD results. For Mn:$CsPbCl_3$ NCs, the Mn^{2+} generally is difficult to dope into the host perhaps because of notable self-purification effect of NCs because the ionic radius of Pb^{2+} is much larger than that of Mn^{2+}. It is known that high-concentration Mn doping at high synthesis temperature or high Mn/Pb ratio will lead to a large amount of defects and traps in NCs, reducing the PL QY.[9,10,19] After introduction of transition metal chlorides such as $NiCl_2$ in this experiment, the Ni doping in NCs and excess Cl ions on the NC surface can effectively suppress defects and trap and improves the crystalline quality in $CsPbCl_3$ NCs,[24−27,61,62] resulting in enhanced doping and emission efficiencies of Mn:$CsPbCl_3$ NCs with respect to the pristine one. This is well consistent with the enhanced formation energies of Mn doping configuration with incorporation of Ni^{2+} estimated by DFT calculation. However, the difference in doping and emission efficiencies of Mn^{2+} in Mn:$CsPbCl_3$ NCs synthesized in the presence of $NiCl_2$, $FeCl_2$, and $CoCl_2$ is not understood. It is necessary to calculate the charge transition levels, defect formation energies, and substituent energy levels in Mn:$CsPbCl_3$ NCs in future work, such as the investigation of partial lead substitution in methylammonium lead bromide.[63]

In summary, we have successfully synthesized Mn and Ni codoped $CsPbCl_3$ perovskite NCs and realized the maximized QYs of Mn^{2+} emissions peaked at 600 and 620 nm as high as 70% and 39%, respectively. The evolution of Mn^{2+} PL lifetimes for Mn:$CsPbCl_3$ NCs with different molar ratios of Mn/Pb and Ni/Pb demonstrated that Ni^{2+} ions are successfully doped into NCs. The suppression of defect and traps states formed in Mn:$CsPbCl_3$ NCs synthesized by introduction of $NiCl_2$ was revealed by variable-temperature PL spectroscopy. The Ni doping in Mn:$CsPbCl_3$ NCs was explained in terms of the enhanced formation energies of Mn doping configuration with incorporation of Ni^{2+} estimated by DFT calculations to improve Mn doping efficiency to boost the Mn^{2+} emission efficiency. It is very interesting to study the photostability of Mn:$CsPbCl_3$ NCs using the transition metal chlorides in a synthetic doping strategy in future work. The orange and red Mn^{2+} emissions in Mn:$CsPbCl_3$ NCs, with their high stability and efficiency, are promising to be used in white LEDs for solid-state lighting.

■ ASSOCIATED CONTENT

Supporting Information

The Supporting Information is available free of charge on the ACS Publications website at DOI: 10.1021/acs.jpclett.9b01588.

Synthesis of Mn:$CsPbCl_3$ NCs with different ratios of Mn/Pb and Ni/Pb; calculation method of PL lifetimes and formation energies of Mn doping configuration; PL spectra, time-resolved PL spectra, QYs, lifetimes, and absorption spectra of Mn:$CsPbCl_3$ NCs; XRD patterns of Ni:$CsPbCl_3$ NCs; synchrotron radiation XRD patterns and PDOS of Mn:$CsPbCl_3$ and (Mn,Ni):$CsPbCl_3$; variable-temperature PL spectra and time-resolved PL spectra of Mn:$CsPbCl_3$ NCs (PDF)

■ AUTHOR INFORMATION

Corresponding Authors

*E-mail: yuanx@jlnu.edu.cn (X.Y.).
*E-mail: zhaojl@ciomp.ac.cn (J.Z.).
*E-mail: lihaibo@jlnu.edu.cn (H.L.).

ORCID

Xi Yuan: 0000-0001-8731-216X
Yi Fan: 0000-0003-0379-9842
Long Yuan: 0000-0002-3047-0295
Zhijian Wu: 0000-0002-8449-8920
Haibo Li: 0000-0001-6108-1965
Jialong Zhao: 0000-0001-9020-1436

Notes

The authors declare no competing financial interest.

■ ACKNOWLEDGMENTS

This work was supported by the National Natural Science Foundation of China (11704152 and 11774134), National Key Research and Development Program of China (2016YFB0401701), Development of Science and Technology of Jilin Province (20190302084GX), and the Thirteenth Five-Year Program for Science and Technology of Education Department of Jilin Province (JJKH20191002KJ).

■ REFERENCES

(1) Liu, W.; Lin, Q.; Li, H.; Wu, K.; Robel, I.; Pietryga, J. M.; Klimov, V. I. Mn^{2+}-Doped Lead Halide Perovskite Nanocrystals with Dual-Color Emission Controlled by Halide Content. *J. Am. Chem. Soc.* **2016**, *138*, 14954−14961.

(2) Parobek, D.; Roman, B. J.; Dong, Y. T.; Jin, H.; Lee, E.; Sheldon, M.; Son, D. H. Exciton-to-Dopant Energy Transfer in Mn-Doped Cesium Lead Halide Perovskite Nanocrystals. *Nano Lett.* **2016**, *16*, 7376−7380.

(3) Liu, H.; Wu, Z.; Shao, J.; Yao, D.; Gao, H.; Liu, Y.; Yu, W.; Zhang, H.; Yang, B. $CsPb_xMn_{1-x}Cl_3$ Perovskite Quantum Dots with High Mn Substitution Ratio. *ACS Nano* **2017**, *11*, 2239−2247.

(4) Guria, A. K.; Dutta, S. K.; Das Adhikari, S.; Pradhan, N. Doping Mn^{2+} in Lead Halide Perovskite Nanocrystals: Successes and Challenges. *ACS Energy Lett.* **2017**, *2*, 1014−1021.

(5) Das Adhikari, S.; Dutta, S. K.; Dutta, A.; Guria, A. K.; Pradhan, N. Chemically Tailoring the Dopant Emission in Manganese-Doped $CsPbCl_3$ Perovskite Nanocrystals. *Angew. Chem., Int. Ed.* **2017**, *56*, 8746−8750.

(6) Huang, G.; Wang, C.; Xu, S.; Zong, S.; Lu, J.; Wang, Z.; Lu, C.; Cui, Y. Postsynthetic Doping of $MnCl_2$ Molecules into Preformed $CsPbBr_3$ Perovskite Nanocrystals Via a Halide Exchange-Driven Cation Exchange. *Adv. Mater.* **2017**, *29*, 1700095.

(7) Xu, K. Y.; Lin, C. C.; Xie, X. B.; Meijerink, A. Efficient and Stable Luminescence from Mn^{2+} in Core and Core-Isocrystalline Shell $CsPbCl_3$ Perovskite Nanocrystals. *Chem. Mater.* **2017**, *29*, 4265−4272.

(8) Rossi, D.; Parobek, D.; Dong, Y. T.; Son, D. H. Dynamics of Exciton-Mn Energy Transfer in Mn-Doped $CsPbCl_3$ Perovskite Nanocrystals. *J. Phys. Chem. C* **2017**, *121*, 17143−17149.

(9) Yuan, X.; Ji, S.; De Siena, M. C.; Fei, L.; Zhao, Z.; Wang, Y.; Li, H.; Zhao, J.; Gamelin, D. R. Photoluminescence Temperature

DOI: 10.1021/acs.jpclett.9b01588
J. Phys. Chem. Lett. 2019, 10, 4177−4184

Dependence, Dynamics, and Quantum Efficiencies in Mn^{2+}-Doped $CsPbCI_3$ Perovskite Nanocrystals with Varied Dopant Concentration. *Chem. Mater.* **2017**, *29*, 8003−8011.
(10) De, A.; Mondal, N.; Samanta, A. Luminescence Tuning and Exciton Dynamics of Mn-doped $CsPbCl_3$ Nanocrystals. *Nanoscale* **2017**, *9*, 16722−16727.
(11) Zhu, J. R.; Yang, X. L.; Zhu, Y. H.; Wang, Y. W.; Cai, J.; Shen, J. H.; Sun, L. Y.; Li, C. Z. Room-Temperature Synthesis of Mn-Doped Cesium Lead Halide Quantum Dots with High Mn Substitution Ratio. *J. Phys. Chem. Lett.* **2017**, *8*, 4167−4171.
(12) Wei, Q.; Li, M. J.; Zhang, Z. P.; Guo, J.; Xing, G. C.; Sum, T. C.; Huang, W. Efficient Recycling of Trapped Energies for Dual-Emission in Mn-Doped Perovskite Nanocrystals. *Nano Energy* **2018**, *51*, 704−710.
(13) Pinchetti, V.; Anand, A.; Akkerman, Q. A.; Sciacca, D.; Lorenzon, M.; Meinardi, F.; Fanciulli, M.; Manna, L.; Brovelli, S. Trap-Mediated Two-Step Sensitization of Manganese Dopants in Perovskite Nanocrystals. *ACS Energy Lett.* **2019**, *4*, 85−93.
(14) Xu, K. Y.; Meijerink, A. Tuning Exciton-Mn^{2+} Energy Transfer in Mixed Halide Perovskite Nanocrystals. *Chem. Mater.* **2018**, *30*, 5346−5352.
(15) Fei, L.; Yuan, X.; Hua, J.; Ikezawa, M.; Zeng, R.; Li, H.; Masumoto, Y.; Zhao, J. Enhanced Luminescence and Energy Transfer in Mn^{2+} doped $CsPbCl_{3-x}Br_x$ Perovskite Nanocrystals. *Nanoscale* **2018**, *10*, 19435−19442.
(16) Chen, D. Q.; Fang, G. L.; Chen, X. Silica-Coated Mn-Doped $CsPb(Cl/Br)_3$ Inorganic Perovskite Quantum Dots: Exciton-to-Mn Energy Transfer and Blue-Excitable Solid-State Lighting. *ACS Appl. Mater. Interfaces* **2017**, *9*, 40477−40487.
(17) Das Adhikari, S.; Guria, A. K.; Pradhan, N. Insights of Doping and the Photoluminescence Properties of Mn-Doped Perovskite Nanocrystals. *J. Phys. Chem. Lett.* **2019**, *10*, 2250−2257.
(18) Swarnkar, A.; Ravi, V. K.; Nag, A. Beyond Colloidal Cesium Lead Halide Perovskite Nanocrystals: Analogous Metal Halides and Doping. *ACS Energy Lett.* **2017**, *2*, 1089−1098.
(19) Das Adhikari, S.; Behera, R. K.; Bera, S.; Pradhan, N. Presence of Metal Chloride for Minimizing the Halide Deficiency and Maximizing the Doping Efficiency in Mn(II)-Doped $CsPbCl_3$ Nanocrystals. *J. Phys. Chem. Lett.* **2019**, *10*, 1530−1536.
(20) Chen, D. Q.; Zhou, S.; Fang, G. L.; Chen, X.; Zhong, J. S. Fast Room-Temperature Cation Exchange Synthesis of Mn-Doped $CsPbCl_3$ Nanocrystals Driven by Dynamic Halogen Exchange. *ACS Appl. Mater. Interfaces* **2018**, *10*, 39872−39878.
(21) Ye, S.; Sun, J. Y.; Han, Y. H.; Zhou, Y. Y.; Zhang, Q. Y. Confining Mn^{2+}-Doped Lead Halide Perovskite in Zeolite-Y as Ultrastable Orange-Red Phosphor Composites for White Light-Emitting Diodes. *ACS Appl. Mater. Interfaces* **2018**, *10*, 24656−24664.
(22) Tang, X.; Chen, W.; Liu, Z.; Du, J.; Yao, Z.; Huang, Y.; Chen, C.; Yang, Z.; Shi, T.; Hu, W.; Zang, Z.; Chen, Y.; Leng, Y. Ultrathin, Core−Shell Structured SiO_2 Coated Mn^{2+}-Doped Perovskite Quantum Dots for Bright White Light-Emitting Diodes. *Small* **2019**, *15*, 1900484.
(23) Wei, Y.; Cheng, Z. Y.; Lin, J. An Overview on Enhancing the Stability of Lead Halide Perovskite Quantum Dots and Their Applications in Phosphor-converted LEDs. *Chem. Soc. Rev.* **2019**, *48*, 310−350.
(24) Wu, Y.; Li, X. M.; Zeng, H. B. Highly Luminescent and Stable Halide Perovskite Nanocrystals. *ACS Energy Lett.* **2019**, *4*, 673−681.
(25) Zheng, X.; Hou, Y.; Sun, H.-T.; Mohammed, O. F.; Sargent, E. H.; Bakr, O. M. Reducing Defects in Halide Perovskite Nanocrystals for Light-Emitting Applications. *J. Phys. Chem. Lett.* **2019**, *10*, 2629−2640.
(26) Zou, S. H.; Liu, Y. S.; Li, J. H.; Liu, C. P.; Feng, R.; Jiang, F. L.; Li, Y. X.; Song, J. Z.; Zeng, H. B.; Hong, M. C.; Chen, X. Y. Stabilizing Cesium Lead Halide Perovskite Lattice through Mn(II) Substitution for Air-Stable Light-Emitting Diodes. *J. Am. Chem. Soc.* **2017**, *139*, 11443−11450.
(27) Pan, G. C.; Bai, X.; Yang, D. W.; Chen, X.; Jing, P. T.; Qu, S. N.; Zhang, L. J.; Zhou, D. L.; Zhu, J. Y.; Xu, W.; Dong, B.; Song, H. W. Doping Lanthanide into Perovskite Nanocrystals: Highly Improved and Expanded Optical Properties. *Nano Lett.* **2017**, *17*, 8005−8011.
(28) Yong, Z. J.; Guo, S. Q.; Ma, J. P.; Zhang, J. Y.; Li, Z. Y.; Chen, Y. M.; Zhang, B. B.; Zhou, Y.; Shu, J.; Gu, J. L.; Zheng, L. R.; Bakr, O. M.; Sun, H. T. Doping-Enhanced Short-Range Order of Perovskite Nanocrystals for Near-Unity Violet Luminescence Quantum Yield. *J. Am. Chem. Soc.* **2018**, *140*, 9942−9951.
(29) Mondal, N.; De, A.; Samanta, A. Achieving Near-Unity Photoluminescence Efficiency for Blue-Violet-Emitting Perovskite Nanocrystals. *ACS Energy Lett.* **2019**, *4*, 32−39.
(30) Bi, C. H.; Wang, S. X.; Li, Q.; Kershaw, S. V.; Tian, J. J.; Rogach, A. L. Thermally Stable Copper(II)-Doped Cesium Lead Halide Perovskite Quantum Dots with Strong Blue Emission. *J. Phys. Chem. Lett.* **2019**, *10*, 943−952.
(31) Zhai, Y.; Bai, X.; Pan, G. C.; Zhu, J. Y.; Shao, H.; Dong, B.; Xu, L.; Song, H. W. Effective Blue-violet Photoluminescence Through Lanthanum and Fluorine Ions Co-doping for $CsPbCl_3$ Perovskite Quantum Dots. *Nanoscale* **2019**, *11*, 2484−2491.
(32) Li, F.; Liu, Y.; Wang, H. L.; Zhan, Q.; Liu, Q. L.; Xia, Z. G. Postsynthetic Surface Trap Removal of $CsPbX_3$ (X = CI, Br, or I) Quantum Dots via a ZnX_2/Hexane Solution toward an Enhanced Luminescence Quantum Yield. *Chem. Mater.* **2018**, *30*, 8546−8554.
(33) Ahmed, G. H.; El-Demellawi, J. K.; Yin, J.; Pan, J.; Velusamy, D. B.; Hedhili, M. N.; Alarousu, E.; Bakr, O. M.; Alshareef, H. N.; Mohammed, O. F. Giant Photoluminescence Enhancement in $CsPbCl_3$ Perovskite Nanocrystals by Simultaneous Dual-Surface Passivation. *ACS Energy Lett.* **2018**, *3*, 2301−2307.
(34) Behera, R. K.; Das Adhikari, S.; Dutta, S. K.; Dutta, A.; Pradhan, N. Blue-Emitting $CsPbCl_3$ Nanocrystals: Impact of Surface Passivation for Unprecedented Enhancement and Loss of Optical Emission. *J. Phys. Chem. Lett.* **2018**, *9*, 6884−6891.
(35) Zhou, Y.; Chen, J.; Bakr, O. M.; Sun, H. T. Metal-Doped Lead Halide Perovskites: Synthesis, Properties, and Optoelectronic Applications. *Chem. Mater.* **2018**, *30*, 6589−6613.
(36) Luo, B. B.; Li, F.; Xu, K.; Guo, Y.; Liu, Y.; Xia, Z. G.; Zhang, J. Z. B-Site Doped Lead Halide Perovskites: Synthesis, Band Engineering, Photophysics, and Light Emission Applications. *J. Mater. Chem. C* **2019**, *7*, 2781−2808.
(37) Wang, J. T. W.; Wang, Z. P.; Pathak, S.; Zhang, W.; deQuilettes, D. W.; Wisnivesky-Rocca-Rivarola, F.; Huang, J.; Nayak, P. K.; Patel, J. B.; Yusof, H. A. M.; Vaynzof, Y.; Zhu, R.; Ramirez, I.; Zhang, J.; Ducati, C.; Grovenor, C.; Johnston, M. B.; Ginger, D. S.; Nicholas, R. J.; Snaith, H. J. Efficient Perovskite Solar Cells by Metal Ion Doping. *Energy Environ. Sci.* **2016**, *9*, 2892−2901.
(38) Gong, X.; Guan, L.; Pan, H. P.; Sun, Q.; Zhao, X. J.; Li, H.; Pan, H.; Shen, Y.; Shao, Y.; Sun, L. J.; Cui, Z. F.; Ding, L. M.; Wang, M. K. Highly Efficient Perovskite Solar Cells via Nickel Passivation. *Adv. Funct. Mater.* **2018**, *28*, 1804286.
(39) Poindexter, J. R.; Hoye, R. L. Z.; Nienhaus, L.; Kurchin, R. C.; Morishige, A. E.; Looney, E. E.; Osherov, A.; Correa-Baena, J. P.; Lai, B.; Bulovic, V.; Stevanovic, V.; Bawendi, M. G.; Buonassisi, T. High Tolerance to Iron Contamination in Lead Halide Perovskite Solar Cells. *ACS Nano* **2017**, *11*, 7101−7109.
(40) Abdi-Jalebi, M.; Andaji-Garmaroudi, Z.; Cacovich, S.; Stavrakas, C.; Philippe, B.; Richter, J. M.; Alsari, M.; Booker, E. P.; Hutter, E. M.; Pearson, A. J.; Lilliu, S.; Savenije, T. J.; Rensmo, H.; Divitini, G.; Ducati, C.; Friend, R. H.; Stranks, S. D. Maximizing and Stabilizing Luminescence from Halide Perovskites with Potassium Passivation. *Nature* **2018**, *555*, 497−501.
(41) Klug, M. T.; Osherov, A.; Haghighirad, A. A.; Stranks, S. D.; Brown, P. R.; Bai, S.; Wang, J. T. W.; Dang, X. N.; Bulovic, V.; Snaith, H. J.; Belcher, A. M. Tailoring Metal Halide Perovskites Through Metal Substitution: Influence on Photovoltaic and Material Properties. *Energy Environ. Sci.* **2017**, *10*, 236−246.
(42) Chen, Y. C.; Chou, H. L.; Lin, J. C.; Lee, Y. C.; Pao, C. W.; Chen, J. L.; Chang, C. C.; Chi, R. Y.; Kuo, T. R.; Lu, C. W.; Wang, D. Y. Enhanced Luminescence and Stability of Cesium Lead Halide

DOI: 10.1021/acs.jpclett.9b01588
J. Phys. Chem. Lett. 2019, 10, 4177−4184

Perovskite $CsPbX_3$ Nanocrystals by Cu^{2+}-Assisted Anion Exchange Reactions. *J. Phys. Chem. C* **2019**, *123*, 2353−2360.
(43) Ding, H. W.; Liu, W. W.; Zheng, Y. K.; Li, C. M.; Jiang, H.; Wang, X. M. Transition Metal Halide-Doped, Highly Stable All-Inorganic Perovskite Nanocrystals for Fabrication of White Light-Emitting Diodes. *J. Mater. Chem. C* **2019**, *7*, 1690−1695.
(44) Kubicki, D. J.; Prochowicz, D.; Pinon, A.; Stevanato, G.; Hofstetter, A.; Zakeeruddin, S. M.; Gratzel, M.; Emsley, L. Doping and Phase Segregation in Mn^{2+}- and Co^{2+}-Doped Lead Halide Perovskites from ^{133}Cs and ^{1}H NMR Relaxation Enhancement. *J. Mater. Chem. A* **2019**, *7*, 2326−2333.
(45) Sampson, M. D.; Park, J. S.; Schaller, R. D.; Chan, M. K. Y.; Martinson, A. B. F. Transition Metal-Substituted Lead Halide Perovskite Absorbers. *J. Mater. Chem. A* **2017**, *5*, 3578−3588.
(46) Williams, S.; Rajagopal, A.; Jo, S. B.; Chueh, C. C.; Tang, T. F. L.; Kraeger, A.; Jen, A. K. Y. Realizing a New Class of Hybrid Organic-Inorganic Multifunctional Perovskite. *J. Mater. Chem. A* **2017**, *5*, 10640−10650.
(47) Dexter, D. L.; Schulman, J. H. Theory of Concentration Quenching in Inorganic Phosphors. *J. Chem. Phys.* **1954**, *22*, 1063−1070.
(48) Barthou, C.; Benoit, J.; Benalloul, P.; Morell, A. Mn^{2+} Concentration Effect on the Optical Properties of Zn_2SiO_4:Mn Phosphors. *J. Electrochem. Soc.* **1994**, *141*, 524−528.
(49) Song, E. H.; Ding, S.; Wu, M.; Ye, S.; Xiao, F.; Zhou, S. F.; Zhang, Q. Y. Anomalous NIR Luminescence in Mn^{2+}-Doped Fluoride Perovskite Nanocrystals. *Adv. Opt. Mater.* **2014**, *2*, 670−678.
(50) Zhang, J. C.; Zhao, L. Z.; Long, Y. Z.; Zhang, H. D.; Sun, B.; Han, W. P.; Yan, X.; Wang, X. S. Color Manipulation of Intense Multiluminescence from CaZnOS:Mn^{2+} by Mn^{2+} Concentration Effect. *Chem. Mater.* **2015**, *27*, 7481−7489.
(51) Nistor, S. V.; Stefan, M.; Nistor, L. C.; Ghica, D.; Vlaicu, I. D.; Joita, A. C. Doping Ultrasmall Cubic ZnS Nanocrystals with Mn^{2+} Ions over a Broad Nominal Concentration Range. *J. Phys. Chem. C* **2015**, *119*, 23781−23789.
(52) Zhou, Q.; Dolgov, L.; Srivastava, A. M.; Zhou, L.; Wang, Z. L.; Shi, J. X.; Dramicanin, M. D.; Brik, M. G.; Wu, M. M. Mn^{2+} and Mn^{4+} Red Phosphors: Synthesis, Luminescence and Applications in WLEDs. A Review. *J. Mater. Chem. C* **2018**, *6*, 2652−2671.
(53) Davis, A. H.; Hofman, E.; Chen, K.; Li, Z. J.; Khammang, A.; Zamani, H.; Franck, J. M.; Maye, M. M.; Meulenberg, R. W.; Zheng, W. W. Exciton Energy Shifts and Tunable Dopant Emission in Manganese-Doped Two-Dimensional CdS/ZnS Core/Shell Nanoplatelets. *Chem. Mater.* **2019**, *31*, 2516−2523.
(54) Senden, T.; van Dijk-Moes, R. J. A.; Meijerink, A. Quenching of the Red Mn^{4+} Luminescence in Mn^{4+}-Doped Fluoride LED Phosphors. *Light: Sci. Appl.* **2018**, *7*, 8.
(55) Yang, X. L.; Pu, C. D.; Qin, H. Y.; Liu, S. J.; Xu, Z. A.; Peng, X. G. Temperature- and Mn^{2+} Concentration-Dependent Emission Properties of Mn^{2+}-Doped ZnSe Nanocrystals. *J. Am. Chem. Soc.* **2019**, *141*, 2288−2298.
(56) Ji, S. H.; Yuan, X.; Li, J.; Hua, J.; Wang, Y. J.; Zeng, R. S.; Li, H. B.; Zhao, J. L. Photoluminescence Lifetimes and Thermal Degradation of Mn^{2+}-Doped $CsPbCl_3$ Perovskite Nanocrystals. *J. Phys. Chem. C* **2018**, *122*, 23217−23223.
(57) Mir, W. J.; Jagadeeswararao, M.; Das, S.; Nag, A. Colloidal Mn-Doped Cesium Lead Halide Perovskite Nanoplatelets. *ACS Energy Lett.* **2017**, *2*, 537−543.
(58) Das Adhikari, S.; Dutta, A.; Dutta, S. K.; Pradhan, N. Layered Perovskites $L_2(Pb_{1-X}Mn_X)C_{14}$ to Mn-Doped $CsPbCl_3$ Perovskite Platelets. *ACS Energy Lett.* **2018**, *3*, 1247−1253.
(59) Dutta, S. K.; Dutta, A.; Das Adhikari, S.; Pradhan, N. Doping Mn^{2+} in Single-Crystalline Layered Perovskite Microcrystals. *ACS Energy Lett.* **2019**, *4*, 343−351.
(60) Locardi, F.; Cirignano, M.; Baranov, D.; Dang, Z. Y.; Prato, M.; Drago, F.; Ferretti, M.; Pinchetti, V.; Fanciulli, M.; Brovelli, S.; De Trizio, L.; Manna, L. Colloidal Synthesis of Double Perovskite $Cs_2AgInCl_6$ and Mn-Doped $Cs_2AgInCl_6$ Nanocrystals. *J. Am. Chem. Soc.* **2018**, *140*, 12989−12995.
(61) De, A.; Das, S.; Mondal, N.; Samanta, A. Highly Luminescent Violet- and Blue-Emitting Stable Perovskite Nanocrystals. *ACS Mater. Lett.* **2019**, *1*, 116−122.
(62) Chen, J.-K.; Ma, J.-P.; Guo, S.-Q.; Chen, Y.-M.; Zhao, Q.; Zhang, B.-B.; Li, Z.-Y.; Zhou, Y.; Hou, J.; Kuroiwa, Y.; Moriyoshi, C.; Bakr, O. M.; Zhang, J.; Sun, H.-T. High-Efficiency Violet-Emitting All-Inorganic Perovskite Nanocrystals Enabled by Alkaline-Earth Metal Passivation. *Chem. Mater.* **2019**, *31*, 3974−3983.
(63) Mannodi-Kanakkithodi, A.; Park, J.-S.; Jeon, N.; Cao, D. H.; Gosztola, D. J.; Martinson, A. B. F.; Chan, M. K. Y. Comprehensive Computational Study of Partial Lead Substitution in Methylammonium Lead Bromide. *Chem. Mater.* **2019**, *31*, 3599−3612.

DOI: 10.1021/acs.jpclett.9b01588
J. Phys. Chem. Lett. 2019, 10, 4177−4184